Eur. Phys. J. C 19, 213–227 (2001)
Digital Object Identifier (DOI) 10.1007/s100520100612

THE EUROPEAN PHYSICAL JOURNAL C

Measurements of $\mathrm{BR}(\mathrm{b} \to \tau^- \bar{\nu}_\tau \mathrm{X})$ and $\mathrm{BR}(\mathrm{b} \to \tau^- \bar{\nu}_\tau \mathrm{D}^{*\pm} \mathrm{X})$ and upper limits on $\mathrm{BR}(\mathrm{B}^- \to \tau^- \bar{\nu}_\tau)$ and $\mathrm{BR}(\mathrm{b} \to \mathrm{s}\nu\bar{\nu})$

The ALEPH Collaboration

R. Barate, D. Decamp, P. Ghez, C. Goy, J.-P. Lees, E. Merle, M.-N. Minard, P. Perrodo, B. Pietrzyk
Laboratoire de Physique des Particules (LAPP), $\mathrm{IN^2P^3}$-CNRS, 74019 Annecy-le-Vieux Cedex, France

S. Bravo, M.P. Casado, M. Chmeissani, J.M. Crespo, E. Fernandez, M. Fernandez-Bosman, Ll. Garrido,[15] E. Graugés, M. Martinez, G. Merino, R. Miquel, Ll.M. Mir, A. Pacheco, A. Pascual, H. Ruiz
Institut de Física d'Altes Energies, Universitat Autònoma de Barcelona, 08193 Bellaterra (Barcelona), Spain[7]

A. Colaleo, D. Creanza, M. de Palma, G. Iaselli, G. Maggi, M. Maggi,[1] S. Nuzzo, A. Ranieri, G. Raso,[23] F. Ruggieri, G. Selvaggi, L. Silvestris, P. Tempesta, A. Tricomi,[3] G. Zito
Dipartimento di Fisica, INFN Sezione di Bari, 70126 Bari, Italy

X. Huang, J. Lin, Q. Ouyang, T. Wang, Y. Xie, R. Xu, S. Xue, J. Zhang, L. Zhang, W. Zhao
Institute of High Energy Physics, Academia Sinica, Beijing, The People's Republic of China[8]

D. Abbaneo, G. Boix,[6] O. Buchmüller, M. Cattaneo, F. Cerutti, G. Dissertori, H. Drevermann, R.W. Forty, M. Frank, T.C. Greening, J.B. Hansen, J. Harvey, P. Janot, B. Jost, I. Lehraus, P. Mato, A. Minten, A. Moutoussi, F. Ranjard, L. Rolandi, D. Schlatter, M. Schmitt,[20] O. Schneider,[2] P. Spagnolo, W. Tejessy, F. Teubert, E. Tournefier, A.E. Wright
European Laboratory for Particle Physics (CERN), 1211 Geneva 23, Switzerland

Z. Ajaltouni, F. Badaud, G. Chazelle, O. Deschamps, A. Falvard, P. Gay, C. Guicheney, P. Henrard, J. Jousset, B. Michel, S. Monteil, J-C. Montret, D. Pallin, P. Perret, F. Podlyski
Laboratoire de Physique Corpusculaire, Université Blaise Pascal, $\mathrm{IN^2P^3}$-CNRS, Clermont-Ferrand, 63177 Aubière, France

J.D. Hansen, J.R. Hansen, P.H. Hansen, B.S. Nilsson, A. Wäänänen
Niels Bohr Institute, 2100 Copenhagen, Denmark[9]

G. Daskalakis, A. Kyriakis, C. Markou, E. Simopoulou, A. Vayaki
Nuclear Research Center Demokritos (NRCD), 15310 Attiki, Greece

A. Blondel,[12] G. Bonneaud, J.-C. Brient, A. Rougé, M. Rumpf, M. Swynghedauw, M. Verderi, H. Videau
Laboratoire de Physique Nucléaire et des Hautes Energies, Ecole Polytechnique, $\mathrm{IN^2P^3}$-CNRS, 91128 Palaiseau Cedex, France

E. Focardi, G. Parrini, K. Zachariadou
Dipartimento di Fisica, Università di Firenze, INFN Sezione di Firenze, 50125 Firenze, Italy

A. Antonelli, M. Antonelli, G. Bencivenni, G. Bologna,[4] F. Bossi, P. Campana, G. Capon, V. Chiarella, P. Laurelli, G. Mannocchi,[5] F. Murtas, G.P. Murtas, L. Passalacqua, M. Pepe-Altarelli[24]
Laboratori Nazionali dell'INFN (LNF-INFN), 00044 Frascati, Italy

A.W. Halley, J.G. Lynch, P. Negus, V. O'Shea, C. Raine, P. Teixeira-Dias, A.S. Thompson
Department of Physics and Astronomy, University of Glasgow, Glasgow G12 8QQ, UK[10]

R. Cavanaugh, S. Dhamotharan, C. Geweniger,[1] P. Hanke, G. Hansper, V. Hepp, E.E. Kluge, A. Putzer, J. Sommer, K. Tittel, S. Werner,[19] M. Wunsch[19]
Kirchhoff-Institut für Physik, Universität Heidelberg, 69120 Heidelberg, Germany[16]

R. Beuselinck, D.M. Binnie, W. Cameron, P.J. Dornan, M. Girone, N. Marinelli, J.K. Sedgbeer, J.C. Thompson,[14] E. Thomson[22]
Department of Physics, Imperial College, London SW7 2BZ, UK[10]

V.M. Ghete, P. Girtler, E. Kneringer, D. Kuhn, G. Rudolph
Institut für Experimentalphysik, Universität Innsbruck, 6020 Innsbruck, Austria[18]

C.K. Bowdery, P.G. Buck, A.J. Finch, F. Foster, G. Hughes, R.W.L. Jones, N.A. Robertson
Department of Physics, University of Lancaster, Lancaster LA1 4YB, UK[10]

I. Giehl, K. Jakobs, K. Kleinknecht, G. Quast,[1] B. Renk, E. Rohne, H.-G. Sander, H. Wachsmuth, C. Zeitnitz
Institut für Physik, Universität Mainz, 55099 Mainz, Germany[16]

A. Bonissent, J. Carr, P. Coyle, O. Leroy, P. Payre, D. Rousseau, M. Talby
Centre de Physique des Particules, Université de la Méditerranée, IN^{2}P^3-CNRS, 13288 Marseille, France

M. Aleppo, F. Ragusa
Dipartimento di Fisica, Università di Milano e INFN Sezione di Milano, 20133 Milano, Italy

H. Dietl, G. Ganis, A. Heister, K. Hüttmann, G. Lütjens, C. Mannert, W. Männer, H.-G. Moser, S. Schael, R. Settles,[1] H. Stenzel, W. Wiedenmann, G. Wolf
Max-Planck-Institut für Physik, Werner-Heisenberg-Institut, 80805 München, Germany[16]

P. Azzurri, J. Boucrot,[1] O. Callot, S. Chen, A. Cordier, M. Davier, L. Duflot, J.-F. Grivaz, Ph. Heusse, A. Jacholkowska,[1] F. Le Diberder, J. Lefrançois, A.-M. Lutz, M.-H. Schune, J.-J. Veillet, I. Videau, C. Yuan, D. Zerwas
Laboratoire de l'Accélérateur Linéaire, Université de Paris-Sud, IN^{2}P^3-CNRS, 91898 Orsay Cedex, France

G. Bagliesi, T. Boccali, G. Calderini, V. Ciulli, L. Foà, A. Giassi, F. Ligabue, A. Messineo, F. Palla,[1] G. Sanguinetti, A. Sciabà, G. Sguazzoni, R. Tenchini,[1] A. Venturi, P.G. Verdini
Dipartimento di Fisica dell'Università, INFN Sezione di Pisa, e Scuola Normale Superiore, 56010 Pisa, Italy

G.A. Blair, G. Cowan, M.G. Green, T. Medcalf, J.A. Strong, J.H. von Wimmersperg-Toeller
Department of Physics, Royal Holloway & Bedford New College, University of London, Surrey TW20 OEX, UK[10]

R.W. Clifft, T.R. Edgecock, P.R. Norton, I.R. Tomalin
Particle Physics Dept., Rutherford Appleton Laboratory, Chilton, Didcot, Oxon OX11 OQX, UK[10]

B. Bloch-Devaux,[1] P. Colas, S. Emery, W. Kozanecki, E. Lançon, M.-C. Lemaire, E. Locci, P. Perez, J. Rander, J.-F. Renardy, A. Roussarie, J.-P. Schuller, J. Schwindling, A. Trabelsi,[21] B. Vallage
CEA, DAPNIA/Service de Physique des Particules, CE-Saclay, 91191 Gif-sur-Yvette Cedex, France[17]

S.N. Black, J.H. Dann, R.P. Johnson, H.Y. Kim, N. Konstantinidis, A.M. Litke, M.A. McNeil, G. Taylor
Institute for Particle Physics, University of California at Santa Cruz, Santa Cruz, CA 95064, USA[13]

C.N. Booth, S. Cartwright, F. Combley, M. Lehto, L.F. Thompson
Department of Physics, University of Sheffield, Sheffield S3 7RH, UK[10]

K. Affholderbach, A. Böhrer, S. Brandt, C. Grupen,[1] A. Misiejuk, G. Prange, U. Sieler
Fachbereich Physik, Universität Siegen, 57068 Siegen, Germany[16]

G. Giannini, B. Gobbo
Dipartimento di Fisica, Università di Trieste e INFN Sezione di Trieste, 34127 Trieste, Italy

J. Rothberg, S. Wasserbaech
Experimental Elementary Particle Physics, University of Washington, Seattle, WA 98195 USA

S.R. Armstrong, K. Cranmer, P. Elmer, D.P.S. Ferguson, Y. Gao, S. González, O.J. Hayes, H. Hu, S. Jin, J. Kile, P.A. McNamara III, J. Nielsen, W. Orejudos, Y.B. Pan, Y. Saadi, I.J. Scott, J. Walsh, Sau Lan Wu, X. Wu, G. Zobernig
Department of Physics, University of Wisconsin, Madison, WI 53706, USA[11]

Received: 2 October 2000 / Published online: 15 March 2001 – © Springer-Verlag 2001

Abstract. Inclusive branching ratios involving b $\to \tau$ transitions are measured in approximately four million hadronic Z decays collected by the ALEPH detector at LEP. The fully-inclusive branching ratio BR(b $\to \tau^-\bar{\nu}_\tau$X) and the semi-inclusive branching ratio BR(b $\to \tau^-\bar{\nu}_\tau$D$^{*\pm}$X) are measured to be $(2.43 \pm 0.20 \pm 0.25)\%$ and $(0.88 \pm 0.31 \pm 0.28)\%$, in agreement with the standard model predictions. Upper limits on the branching fractions BR(B$^-$ $\to \tau^-\bar{\nu}_\tau$) and BR(b $\to$ s$\nu\bar{\nu}$) are set to 8.3×10^{-4} and 6.4×10^{-4} at the 90% C.L. These results allow a 90% C.L. lower limit of 0.40 (GeV/c^2)$^{-1}$ to be set on the $\tan\beta/m_{\mathrm{H}^\pm}$ ratio, in the framework of type-II two-Higgs-doublet models.

1 Introduction

Third-generation fermions are involved in both the initial and final states of b $\to \tau$ transitions. A measurement of branching ratios pertaining to these transitions can be compared to the standard model predictions, yielding direct tests of heavy fermion interactions. These interactions are especially sensitive to the mechanism underlying the electroweak symmetry breaking, *i.e.*, to the origin of mass, and allow extensions of the standard model to be constrained in this respect. In the study presented here, the branching fractions of the following processes are considered.

- The inclusive branching fraction BR(b $\to \tau^-\bar{\nu}_\tau$X) can be compared to the standard model prediction of $2.30 \pm 0.25\%$[1], as computed in the framework of the Heavy Quark Effective Theory (HQET). The standard model transition, illustrated in Fig. 1a, could be modified by the exchange of a new charged boson, as shown in Fig. 1b with a charged Higgs boson. In any type-II two-Higgs-doublet model, such as the minimal supersymmetric extension of the standard model, the corresponding contribution to the transition amplitude is proportional to $(\tan\beta/m_{\mathrm{H}^\pm})^2$ [2–4], where $\tan\beta$ is the ratio of the vacuum expectation values of the two Higgs doublets, and $m_{\mathrm{H}^\pm}$ is the mass of the charged Higgs boson.

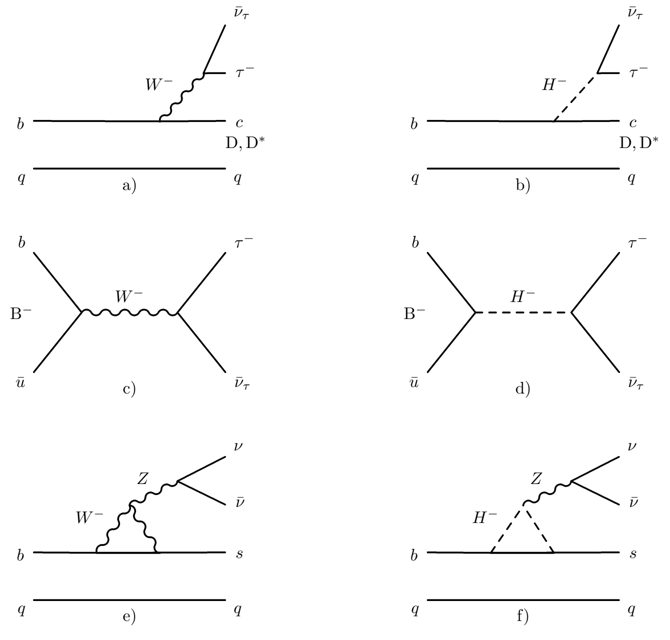

Fig. 1a–f. Feynman graphs for the processes b $\to \tau^-\bar{\nu}_\tau$X, B$^-$ $\to \tau^-\bar{\nu}_\tau$ and b $\to$ s$\nu\bar{\nu}$, in the standard model **a**, **c**, **e** and in two-Higgs-doublet models with the exchange of a charged Higgs boson **b**, **d**, **f**

- A similar test can be performed with the semi-inclusive decay b $\to \tau^-\bar{\nu}_\tau$D^{*+}X. In the standard model, this branching fraction is expected to be approximately 1% [5]. The proportion of D* relative to D final states would be reduced in the presence of a charged Higgs boson [6].
- The exclusive decay mode B$^-$ $\to \tau^-\bar{\nu}_\tau$ (Fig. 1c) has a branching fraction predicted to be $7.4 \times 10^{-5}(f_{\mathrm{B}}/160\,\mathrm{MeV})^2\,(|\mathrm{V_{ub}}|/0.004)^2$ in the standard model [7]. In type-II two-Higgs-doublet models (Fig. 1d), the rate is enhanced [7] by the multiplicative factor $[m^2_{\mathrm{B}^-}(\tan\beta/m_{\mathrm{H}^\pm})^2 - 1]^2$.
- Although it does not involve a b $\to \tau$ transition, the decay b $\to$ s$\nu\bar{\nu}$, with a branching fraction predicted to be of the order of 5×10^{-5} in the standard model (Fig. 1e), can also be exploited to put constraints on a variety of extensions of the standard model (Fig. 1f) as advocated in [8,9].

---

[1] Also at CERN, 1211 Geneva 23, Switzerland

[2] Now at Université de Lausanne, 1015 Lausanne, Switzerland

[3] Also at Dipartimento di Fisica di Catania and INFN Sezione di Catania, 95129 Catania, Italy

[4] Also Istituto di Fisica Generale, Università di Torino, 10125 Torino, Italy

[5] Also Istituto di Cosmo-Geofisica del C.N.R., Torino, Italy

[6] Supported by the Commission of the European Communities, contract ERBFMBICT982894

[7] Supported by CICYT, Spain

[8] Supported by the National Science Foundation of China

[9] Supported by the Danish Natural Science Research Council

[10] Supported by the UK Particle Physics and Astronomy Research Council

[11] Supported by the US Department of Energy, grant DE-FG0295-ER40896

[12] Now at Departement de Physique Corpusculaire, Université de Genève, 1211 Genève 4, Switzerland

[13] Supported by the US Department of Energy, grant DE-FG03-92ER40689

[14] Also at Rutherford Appleton Laboratory, Chilton, Didcot, UK

[15] Permanent address: Universitat de Barcelona, 08208 Barcelona, Spain

[16] Supported by the Bundesministerium für Bildung, Wissenschaft, Forschung und Technologie, Germany

[17] Supported by the Direction des Sciences de la Matière, C.E.A

[18] Supported by the Austrian Ministry for Science and Transport

[19] Now at SAP AG, 69185 Walldorf, Germany

[20] Now at Harvard University, Cambridge, MA 02138, U.S.A

[21] Now at Département de Physique, Faculté des Sciences de Tunis, 1060 Le Belvédère, Tunisia

[22] Now at Department of Physics, Ohio State University, Columbus, OH 43210-1106, U.S.A

[23] Also at Dipartimento di Fisica e Tecnologie Relative, Università di Palermo, Palermo, Italy

[24] Now at CERN, 1211 Geneva 23, Switzerland

The measurements of the branching fractions of these four processes, $\mathrm{b} \to \tau^- \bar{\nu}_\tau \mathrm{X}$, $\mathrm{b} \to \tau^- \bar{\nu}_\tau \mathrm{D}^{*\pm} \mathrm{X}$, $\mathrm{B}^- \to \tau^- \bar{\nu}_\tau$ and $\mathrm{b} \to \mathrm{s}\nu\bar{\nu}$, are performed with all data collected by the ALEPH detector between 1991 and 1995, at centre-of-mass energies at and around the Z resonance, corresponding to approximately four million hadronic Z decays. As described in previous ALEPH studies applied to smaller data samples [10,11], a single technique is used to extract the four branching ratios. The initial-state b quark is identified by means of standard b-tagging algorithms, and the final-state τ lepton (or the two neutrinos in the case of $\mathrm{b} \to \mathrm{s}\nu\bar{\nu}$) is identified by the missing energy carried away by the neutrinos.

The energy-flow and b-tagging algorithms are briefly described in Sect. 2 along with properties of the ALEPH detector relevant for the present study. The selection algorithms aimed at rejecting background events with a large missing energy are presented in Sect. 3. The method to estimate the residual background yields is detailed in Sect. 4. The branching ratios BR($\mathrm{b} \to \tau^- \bar{\nu}_\tau \mathrm{X}$) and BR($\mathrm{b} \to \tau^- \bar{\nu}_\tau \mathrm{D}^{*\pm} \mathrm{X}$) are determined in Sect. 5, and the limits on BR($\mathrm{B}^- \to \tau^- \bar{\nu}_\tau$) and BR($\mathrm{b} \to \mathrm{s}\nu\bar{\nu}$) are extracted in Sect. 6. Finally, an alternative measurement of BR($\mathrm{b} \to \tau^- \bar{\nu}_\tau \mathrm{X}$) with opposite-sign di-leptons in the final state is presented in Sect. 7. The results are interpreted in the framework of type-II two-Higgs-doublet models in Sect. 8 and summarized in Sect. 9.

2 The ALEPH Detector

A detailed description of the ALEPH detector can be found in [12], and of its performance in [13]. Charged particles are detected in the central part, consisting of a precision silicon vertex detector, a cylindrical drift chamber and a large time projection chamber, measuring altogether up to 31 space points along the charged particle trajectories. A 1.5 T axial magnetic field is provided by a superconducting solenoidal coil. Charged particle transverse momenta are reconstructed with a $1/p_T$ resolution of $\left(6 \times 10^{-4} \bigoplus 5 \times 10^{-3}/p_T\right)$ $(\mathrm{GeV}/c)^{-1}$. In the following, *good* tracks are defined as charged particle tracks reconstructed with at least four hits in the time projection chamber, originating from within a cylinder of length 20 cm and radius 2 cm coaxial with the beam and centred at the nominal collision point, and with a polar angle with respect to the beam such that $|\cos\theta| < 0.95$.

Jets originating from b quarks are identified with a lifetime b-tagging algorithm [14], which takes advantage of the three-dimensional impact parameter resolution of charged particle tracks. For tracks with two space points in the silicon vertex detector (*i.e.*, $|\cos\theta| < 0.7$), this resolution can be parametrized as $(25 + 95/p)$ μm, with p in GeV/c.

In addition to its rôle as a tracking device, the time projection chamber also measures the specific energy loss by ionization $\mathrm{d}E/\mathrm{d}x$. It allows low momentum electrons to be separated from other charged particle species by more than three standard deviations.

Electrons (and photons) are also identified by the characteristic longitudinal and transverse developments of the associated showers in the electromagnetic calorimeter, a 22 radiation length thick sandwich of lead planes and proportional wire chambers with fine read-out segmentation. The relative energy resolution achieved is $0.18/\sqrt{E}$ (E in GeV) for isolated electrons and photons.

Photon conversions to $\mathrm{e}^+\mathrm{e}^-$ in the detector material are identified as a pair of oppositely charged identified electrons satisfying the following conditions: *(i)* the distance of closest approach to the beam of the two reconstructed tracks is larger than 2 mm; *(ii)* the distance between the two tracks at their point of closest approach is smaller than 2 cm in space; *(iii)* the position of this point is consistent with a material boundary; and *(iv)* the invariant mass is smaller than 20 MeV/c^2, when calculated as for an $\mathrm{e}^+\mathrm{e}^-$ pair coming from this point of closest approach.

Muons are identified by their characteristic penetration pattern in the hadron calorimeter, a 1.5 m thick yoke interleaved with 23 layers of streamer tubes, together with two surrounding double-layers of muon chambers. In association with the electromagnetic calorimeter, the hadron calorimeter also provides a measurement of the hadronic energy with a relative resolution of $0.85/\sqrt{E}$ (E in GeV).

Taus are identified by the missing energy carried away by their decay neutrinos. The total visible energy is measured with an energy-flow reconstruction algorithm which combines all the above measurements, supplemented by the energy detected at low polar angle (down to 24 mrad from the beam axis) by two additional electromagnetic calorimeters, used for the luminosity determination. The relative resolution on the total visible energy varies between $0.60/\sqrt{E}$ for high multiplicity final states and $0.25/\sqrt{E}$ for final states of low multiplicity without neutral hadrons. In addition to the total visible-energy measurement, the energy-flow reconstruction algorithm also provides a list of reconstructed objects, classified as charged particles, photons and neutral hadrons, and called *energy-flow particles* in the following.

3 Event selections

A $\mathrm{b} \to \tau$ transition followed by the decay of the τ always produces two energetic ν_τ's. Such transitions can therefore be identified in $\mathrm{e}^+\mathrm{e}^- \to \mathrm{b}\bar{\mathrm{b}}$ events on the basis of a large measured missing energy. The argument holds as well for $\mathrm{b} \to \mathrm{s}\nu\bar{\nu}$ decays, which can be selected along the same lines as $\mathrm{b} \to \tau$ transitions. In this section, the algorithms aimed at rejecting background events leading to large measured missing energy are described. An alternative selection, based on the presence of two identified leptons with opposite electric charge, is described in Sect. 7.

3.1 Preselection

Approximately four million hadronic Z decays are selected in the data collected between 1991 and 1995 at energies at and around the Z resonance when the standard criteria (at least five good tracks carrying at least 10% of the centre-of-mass energy [15]) are applied. To keep only two-jet events well contained in the detector acceptance, the polar angle is required to satisfy $|\cos\theta_{\mathrm{thrust}}| < 0.7$ to match the acceptance of the vertex detector, and the thrust value must exceed 0.85.

Each event is then divided in two hemispheres with respect to the plane perpendicular to the thrust axis. In each hemisphere, the missing energy $E_{\mathrm{miss}}^{1,2}$ is defined as the difference between the expected true energy $E_{\mathrm{true}}^{1,2}$ and the measured visible energy $E_{\mathrm{vis}}^{1,2}$. The latter is determined from the total energy of all energy-flow particles contained in that hemisphere, while the former is estimated from the centre-of-mass energy $\sqrt{s}$ and with energy-momentum conservation: $E_{\mathrm{true}}^{1,2} = (s + m_{1,2}^2 - m_{2,1}^2)/2\sqrt{s}$, where m_1 and m_2 are the measured invariant masses in the two hemispheres [16].

The main background to the final states searched for in this analysis consists of $Z \to b\bar{b}$ or $c\bar{c}$ events followed by a semi-leptonic b or c decay into an electron or a muon (hereafter called lepton and denoted ℓ), with a large missing energy carried away by the neutrino ν_ℓ. This background can be considerably reduced by rejecting hemispheres in which a lepton is identified. The standard lepton identification [17] is not used here, but is replaced by much looser criteria. A good track is tagged as an electron either if the $\mathrm{d}E/\mathrm{d}x$ is compatible with that of an electron and incompatible with that of a pion, or if the transverse and longitudinal profiles of the associated electromagnetic shower are compatible with those of an electron. Electrons and positrons originating from identified photon conversions are not considered in this process. Similarly, a good track is tagged as a muon if it is associated to a few hits either in the last layers of the hadron calorimeter or in the two layers of muon chambers. A lepton identification efficiency over 95% is achieved for electrons (muons) with a momentum in excess of 1 (2) GeV/c.

In addition, to reduce the contamination from Z decays into lighter quark pairs ($u\bar{u}$, $d\bar{d}$, $s\bar{s}$ and $c\bar{c}$) in which a large missing energy is faked due to finite detector resolution effects, the final sample is enriched in $Z \to b\bar{b}$ events with b tagging. The corresponding criteria are dependent on the signal final state and are described in the following subsections.

3.2 The $b \to \tau^- \bar{\nu}_\tau X$ final state

For the $b \to \tau^- \bar{\nu}_\tau X$ final state selection, a hemisphere is kept only if the opposite hemisphere is tagged as arising from a b quark. Each good track in the opposite hemisphere is assigned a probability of originating from the primary interaction point, on the basis of its impact parameter significance. The confidence level α^{hemi} that all good tracks in that hemisphere come from the primary interaction point, determined under the assumption that the individual probabilities are uncorrelated [14], is required to be smaller than 1%.

Residual backgrounds like $Z \to \tau^+\tau^-$ decays, two-photon processes or beam-gas interactions are likely to yield a large missing energy in the final state and might therefore bias the analysis. These background sources are reduced down to negligible levels by requiring at least seven good tracks and a total missing energy smaller than 50 GeV, with almost no additional loss of the signal.

3.3 The $B^- \to \tau^- \bar{\nu}_\tau$ and $b \to s\nu\bar{\nu}$ final states

The same b-tagging technique as for the $b \to \tau^- \bar{\nu}_\tau X$ selection is applied but the residual backgrounds are rejected in a slightly different manner. The opposite hemisphere is required to contain at least six good tracks, and its missing energy must be smaller than 25 GeV. This latter cut reduces the effect on the missing-energy distribution in the signal hemisphere, which is expected to extend towards larger values than in the previous case.

3.4 The $b \to \tau^- \bar{\nu}_\tau D^{*\pm} X$ final state

The $b \to \tau^- \bar{\nu}_\tau D^{*\pm} X$ final state selection is primarily based on an exclusive reconstruction of a $D^{*\pm}$, very similar to that performed in [18] although with slightly tighter cuts as a result of the larger statistics accumulated until 1995.

Candidate $D^{*\pm}$'s are searched for in the decay channel $D^{*\pm} \to D^0\pi_{\mathrm{soft}}$, followed by $D^0 \to K^-\pi^+\pi^-\pi^+$, $D^0 \to K^-\pi^+$, $D^0 \to K^-\pi^+\pi^0$ or $D^0 \to K_S^0\pi^+\pi^-$, selected as follows.

Neutral pions are identified as photon pairs with an invariant mass compatible with the π^0 mass and a χ^2 probability in excess of 1%. Candidate K_S^0's are identified as pairs of oppositely charged particle tracks (assumed to be charged pions) forming a secondary vertex at least 2 cm away from the primary interaction point, and with a reconstructed invariant mass within 5 MeV/c^2 of the K_S^0 mass. Candidate $K^\pm$'s are identified as good tracks of momentum in excess of 3 GeV/c and with a $\mathrm{d}E/\mathrm{d}x$ compatible with that of a charged kaon within two standard deviations. In addition the angle θ^* between the kaon momentum direction, evaluated in the D^0 rest frame, and the D^0 line-of-flight must satisfy $|\cos\theta^*| < 0.9$.

The reconstructed invariant mass of the candidate D^0's is required to be within 15 MeV/c^2 (50 MeV/c^2) of the D^0 mass for the first (last) two decay channels. The ratio of the D^0 energy to the beam energy is required to be between 0.25 and 0.50. In addition, the reconstructed D^0 vertex must be incompatible with the primary interaction point by at least two standard deviations.

Each reconstructed D^0 is associated with a low momentum pion ($p_{\pi_{\mathrm{soft}}} < 4.2$ GeV/c) to form a $D^{*\pm}$. The reconstructed invariant mass difference $m_{D^{*\pm}} - m_{D^0}$ is required to be within 20 MeV/c^2 of the nominal mass difference.

Finally, the $D^{*\pm}$ hemispheres are tagged as arising from a b quark by requiring the presence of an additional good track in a cone of half-angle 30° around the

D^0 momentum direction. This track must be incompatible with originating from the primary interaction point by more than three standard deviations, and its electric charge must be opposite to that of the π_{soft}. No b tagging needs therefore be applied to the opposite hemisphere.

3.5 Event yields

The expected event yields were determined with the following samples of events, simulated with `JETSET` [19,20], and subsequently processed through the full `GEANT` [21] simulation of the detector:

- approximately four million hadronic Z decays for the background estimate;
- over 40 000 $b\bar{b}$ events, each containing a $b \to \tau^- \bar{\nu}_\tau X$, with the τ polarization determined in the limit of the free-quark model [1] for $m_b = 4.8\,\mathrm{GeV}/c^2$ and $m_c = 1.4\,\mathrm{GeV}/c^2$;
- about 20 000 $b\bar{b}$ events with at least one $B^- \to \tau^- \bar{\nu}_\tau$ and 100% polarized τ's;
- almost 20 000 $b\bar{b}$ events with at least one $b \to s\nu\bar{\nu}$, generated with the $B \to X_s \nu\bar{\nu}$ decay probability given in [8], in which the new-physics parameters were conservatively chosen to minimize the expected selection efficiency. The model was improved with a realistic X_s invariant mass distribution, described as a Gaussian of mean and variance 1.35 and $0.60\,\mathrm{GeV}/c^2$[9], supplemented by two peaks at the K and K^* masses [22] with branching fractions of 0.06 ± 0.02 and 0.29 ± 0.01.

In all these samples, the polarization of the τ's was properly taken into account in the simulation of their decay kinematics [23], and events containing a Λ_b were reweighted according to the measured Λ_b polarization [24], so that the correct distribution of the ν_τ momenta, and therefore the missing energy, be obtained.

The numbers of hemispheres expected to be selected from the various background and signal processes and the numbers of hemispheres selected in the data are listed in Table 1.

The measurement of the various branching fractions relies on the observation of an excess of events at large E_{miss} in the missing-energy distribution of the data with respect to that of the simulated background. Given the limited number of events expected from the various signal processes (Table 1), it is essential to have a detailed understanding of all uncertainties affecting the background distribution both in shape and normalization (Sect. 4) and of the signal selection efficiencies (Sect. 5).

Table 1. Numbers of hemispheres selected in the data in the four different final states. Also indicated are the numbers of hemispheres expected from the various background and signal processes. For the latter, the standard model branching ratio values were assumed. The standard model branching ratios and the selection efficiencies are indicated in brackets

Final state selection	$\tau^- \bar{\nu}_\tau X$	$\tau^- \bar{\nu}_\tau D^{*\pm} X$	$\tau^- \bar{\nu}_\tau$, $s\nu\bar{\nu}$
Data			
Hemispheres selected	166342	1464	156910
Simulation			
Hemispheres expected	162456	1538	153093
Background (details)			
u, d, s	9215	1172	8855
b, c without leptonic decay	138118	80	129886
b, c with leptonic decay	10645	180	10091
Signal (details)			
$b \to \tau^- \bar{\nu}_\tau X$ (2.3%)	(12%) 4478	–	4247
$b \to \tau^- \bar{\nu}_\tau D^{*\pm} X$ (1.0%)	–	(0.34%) 81	–
$b \to \tau^- \bar{\nu}_\tau X$ without $D^{*\pm}$	–	25	–
$B^- \to \tau^- \bar{\nu}_\tau$ (7.4×10^{-5})	–	–	(8.1%) 4
$b \to s\nu\bar{\nu}$ (5.0×10^{-5})	–	–	(8.8%) 10

4 Background estimate

The missing-energy distribution of the background to $b \to \tau$ and $b \to s\nu\bar{\nu}$ transitions depends on detector performance in three areas, *(i)* the visible-energy reconstruction for hemispheres with *a priori* no missing energy such as Z hadronic decays into light-quark pairs; *(ii)* the effectiveness of the lepton veto to reject background from $b, c \to \ell \nu_\ell X$; and *(iii)* the performance of the b-tagging. To minimize the influence of possible inaccuracies in the detector simulation, these three quantities are derived from the data and subsequently used to re-weight the simulated events.

4.1 The visible-energy calibration

As mentioned above, the accuracy of the visible-energy reconstruction can be studied with a sample of events in which no significant missing energy is expected. Such a sample is selected in a way identical to that followed in Sects. 3.1 and 3.2 except that the b-tagging criterion is replaced by a b-rejection one requiring $\alpha^{\mathrm{hemi}} > 0.5$. It yields fractions of 88.7%, 10.5% and 0.8% for ($u\bar{u}$,$d\bar{d}$,$s\bar{s}$), $c\bar{c}$ and $b\bar{b}$ events, respectively.

The visible energy E_{vis} is the sum of the energy E_{cha} of the charged particles reconstructed in the central tracker, the energy E_{pho} of the photons detected in the electromagnetic calorimeter, and the energy E_{neu} of the neutral hadrons, the reconstruction of which makes use of all identification and energy measurement capabilities of the detector (Sect. 2). These three contributions to the visible energy may therefore be affected by different systematic uncertainties and must be calibrated separately. The hemispheres were thus binned in a grid according to the fractional contributions to the visible energy of the charged, photon and neutral hadron components ($E_{\mathrm{cha}}/E_{\mathrm{vis}}$, $E_{\mathrm{pho}}/E_{\mathrm{vis}}$, $E_{\mathrm{neu}}/E_{\mathrm{vis}}$). The accuracy of the detector simulation was examined by comparing the observed and simulated missing energy in each of the bins.

Table 2. Calibration parameters (see text for a detailed description) for E_{vis}

f_{cha}	1.002 ± 0.001
f_{pho}	1.000 ± 0.002
f_{neu}	0.936 ± 0.010
f_{b}	0.999 ± 0.001

A noticeable inaccuracy of the simulation was found in hemispheres with a large proportion of neutral hadronic energy. This disagreement with the data could lead to a large systematic uncertainty in the final result. Moreover, the neutral hadronic energy is expected to be smaller in $\text{b}\bar{\text{b}}$ events than in other hadronic Z decays. It was therefore decided to reject all hemispheres for which E_{neu} is in excess of 7 GeV, both in this calibration procedure and in the selections described in the previous section, preserving 69.6% of the events in the data and 68.7% in the simulation.

The residual differences between the data and the simulation were corrected by scaling E_{cha}, E_{pho} and E_{neu} by f_{cha}, f_{pho} and f_{neu}, respectively, in the simulated events. The values of these calibration factors were obtained by minimizing the following χ^2,

$$\chi^2 = \sum_i \left\{ \langle E^{\text{data}}_{\text{vis,i}} \rangle - \left[f_{\text{cha}} \langle E^{\text{MC}}_{\text{cha},i} \rangle + f_{\text{pho}} \langle E^{\text{MC}}_{\text{pho},i} \rangle \right.\right.$$
$$\left.\left. + f_{\text{neu}} \langle E^{\text{MC}}_{\text{neu},i} \rangle \right] \right\}^2 / \sigma_i^2, \qquad (1)$$

where the mean energy values are computed in each bin i, $E^{\text{data}}_{\text{vis},i}$ is the total visible energy measured in that bin, the $E^{\text{MC}}_{\text{xxx},i}$ values are the charged, photonic and neutral hadronic energies expected in that bin, and σ_i is the uncertainty due to the limited statistics of the event samples. The result of the fit is shown in Table 2. While f_{cha} and f_{pho} are compatible with unity, a sizeable calibration is found to be still necessary for the neutral hadronic energy, despite the cut at 7 GeV. This effect, already reported in [10], results from an inadequacy of the simulation of nuclear interactions.

As another consequence, the E_{neu} resolution is better in the simulation than in the data. In addition to the rescaling, the simulated neutral hadronic energy was therefore smeared on an event-by-event basis, leading to a $(1.1 \pm 1.6)\%$ relative deterioration of the E_{neu} resolution. This smearing was performed in order to equalize the observed and expected numbers of events with a reconstructed E_{miss} in excess of 14 GeV. Indeed, in events where no real missing energy is expected, such a large reconstructed E_{miss} value is often due to a loss of neutral hadronic energy.

The distributions of the reconstructed missing energy in the control sample are displayed in Fig. 2, both for data and simulated events, before and after the calibration procedure. The agreement is found to be adequate over the whole spectrum, and in particular at large missing energy where the background to the signal of interest in this paper has to be evaluated.

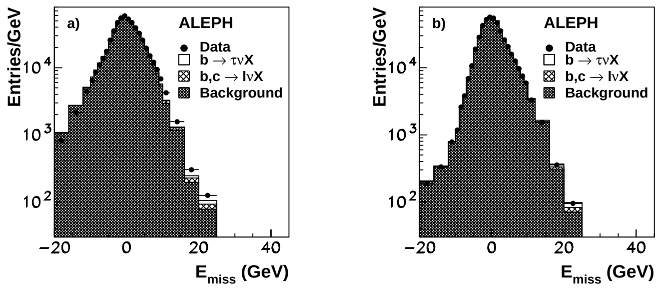

Fig. 2a,b. Reconstructed missing-energy distributions using the light-quark tag and e/μ veto **a** before calibration; **b** after missing-energy recalibration and applying the cut $E_{\text{neu}} <$ 7 GeV

Finally, due to the specific hadronization and fragmentation of b-quark jets, the sharing between the charged, photonic and neutral hadronic energy may lead to an overall visible-energy shift different from that observed for lighter quark species. The visible energy of hemispheres tagged as arising from a b quark was therefore rescaled by an overall factor f_{b}, determined from the b-tagged sample of Sect. 3.2 so as to match the peak positions (which are not affected by events with truly missing energy) of the expected and observed visible-energy distributions. This b-specific calibration factor is found to be compatible with unity (Table 2).

4.2 The lepton rejection effectiveness

In order to estimate the effectiveness of the lepton veto, aimed at rejecting $\text{Z} \to \text{b}\bar{\text{b}}$ or $\text{c}\bar{\text{c}}$ events followed by a semi-leptonic b or c decay into an electron or a muon, the veto was applied to unbiased, pure, lepton data and simulated samples.

A 97.6% pure electron sample was obtained by selecting hadronic events with a photon conversion, as described in Sect. 2, in which only one of the two particles has to be identified as an electron. Photon conversions are well suited to study the electron veto since the hadronic environment is very similar to that of semi-leptonic heavy-flavour decays. The electron-veto effectiveness is thus given by the probability, after background subtraction, that the second particle be identified as an electron by the lepton-veto criteria. However, this probability depends on *(i)* the electron momentum, the spectrum of which is different in photon conversions and in semi-leptonic b/c decays; and *(ii)* the number of wires used for the dE/dx measurement, which tends to be smaller in photon conversions than in semi-leptonic b/c decays due to shared hits with the first electron of the converted pair. Therefore, the electron identification probability was mapped as a function of the electron momentum and the number of hits associated to the corresponding track, both for the data and the simulated events with photon conversions. The ratio of these two maps was then used to re-weight the simulated b/c events with semi-leptonic decays.

For the muons, a sample originating from the $\gamma\gamma \to \mu^+\mu^-$ process was selected. The absence of hadronic en-

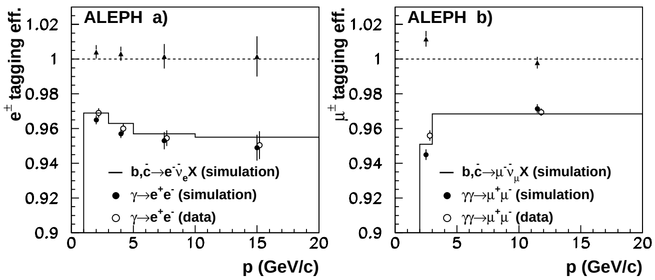

Fig. 3a,b. Lepton identification efficiencies **a** for electrons and **b** for muons as a function of momentum in the control samples (see text) for the data (open circles) and the simulation (full circles), and their ratio (triangles). The histograms show the identification efficiency for simulated b/c events with semi-leptonic decays

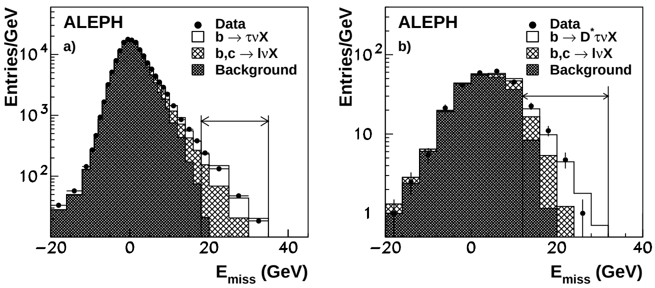

Fig. 4a,b. Missing-energy distributions in the b → $\tau^-\bar{\nu}_\tau$X **a** and the b → $\tau^-\bar{\nu}_\tau$D$^{*\pm}$X **b** final states, for the data (dots) and the simulation (histograms). The latter is subdivided in *(i)* the fitted signal contribution (empty histogram); *(ii)* the contribution from b and c semi-leptonic decays (light hatching); and *(iii)* the residual background (dark hatching). Also indicated are the E_{miss} intervals considered for the branching ratio measurements (Sect. 5.1)

vironment is less important because the identification is achieved with the external layers of the hadron calorimeter and the muon chambers. A 97.1% pure sample of low-momentum muons was obtained by requiring exactly two good tracks (accompanied by no neutral energy-flow particle) with opposite electric charge, one of which being identified as a muon, a total momentum less than 30 GeV/c and an invariant mass smaller than 2 GeV/c^2. Above 3 GeV/c, muons are expected to traverse entirely the hadron calorimeter and the muon chambers, making the identification efficiency independent of momentum. The $\gamma\gamma \to \mu^+\mu^-$ sample was therefore supplemented by Z decays into muon pairs to determine the latter. As above, and after background subtraction, the muon-veto effectiveness was given by the probability that the second particle be identified as a muon by the lepton-veto criteria as a function of momentum, both in the data and in the simulation. The ratio was then used to re-weight the simulated b/c events with semi-leptonic decays.

The identification probability for electrons and muons, determined from these samples, is displayed as a function of the lepton momentum in Figs. 3a and 3b, for data and simulation, and is compared to the identification efficiency for simulated b/c events with semi-leptonic decays. The data-to-simulation ratio, applied as a correction factor to the latter, is consistently found to be close to unity.

4.3 The b-tagging efficiency

The efficiency of the b-tagging criterion can be determined directly from the data using the double tag method [14], so as to minimize the systematic uncertainties related to the limited knowledge of b-hadron production and decay. The small correlation between the b-tagging probabilities in the two hemispheres is negligible for the present purpose.

From the knowledge of the fractions R_{b} and R_{c} of hadronic Z decays into b$\bar{\mathrm{b}}$ and c$\bar{\mathrm{c}}$, the efficiencies ε_{b} and ε_{c} of the b-tagging criterion on b and c hemispheres can be measured in the data by comparing the fraction f_1 of hemispheres which pass a given α^{hemi} cut with the fraction f_2 of events in which both hemispheres pass the same cut. These fractions are given by

$$\begin{aligned} f_1 &= R_{\mathrm{b}}\varepsilon_{\mathrm{b}} + R_{\mathrm{c}}\varepsilon_{\mathrm{c}} + (1 - R_{\mathrm{c}} - R_{\mathrm{b}})\varepsilon_{\mathrm{x}}, \\ f_2 &= R_{\mathrm{b}}\varepsilon_{\mathrm{b}}^2 + R_{\mathrm{c}}\varepsilon_{\mathrm{c}}^2 + (1 - R_{\mathrm{c}} - R_{\mathrm{b}})\varepsilon_{\mathrm{x}}^2, \end{aligned} \tag{2}$$

where ε_{x} is the hemisphere tagging efficiency for light-quark hemispheres, the value of which is determined directly with the data as explained in [14]. The difference between the observed and expected ε_{x} values for a given α^{hemi} cut arises from from different impact parameter resolutions in the data and in the simulation. This difference was estimated from the fraction of hemispheres satisfying $\alpha^{\mathrm{hemi}}_{\mathrm{neg}} < 0.01$, where $\alpha^{\mathrm{hemi}}_{\mathrm{neg}}$ is the hemisphere probability recomputed with only those tracks having negative impact parameter (and reversing the impact parameter sign). Such tracks nearly always originate from the primary vertex, and account for resolution differences. The relatively small contribution of long-lived particles (such as $\mathrm{K}^0_{\mathrm{S}}$ or Λ^0) is taken from the simulation.

With the cut $\alpha^{\mathrm{hemi}} < 0.01$, ε_{x} was found to be 2.46%, *i.e.*, slightly larger in the data than predicted by the simulation by a factor of 1.17±0.11. With the ε_{x} value obtained this way, (2) was solved for ε_{b} and ε_{c}. The tagging efficiencies for b (56.7%) and c (14.8%) hemispheres were also found to be larger in the data by factors of 1.03 ± 0.01 and 1.03 ± 0.03, respectively, and were used to re-weight the simulated events accordingly.

5 Measurement of b → $\tau^-\bar{\nu}_\tau$X and b → $\tau^-\bar{\nu}_\tau$D$^{*\pm}$X

The b → $\tau^-\bar{\nu}_\tau$X and b → $\tau^-\bar{\nu}_\tau$D$^{*\pm}$X branching fractions can be determined by evaluating the excess of events over the background expected at large missing energy from the two selections (Sects. 3.2 and 3.4). The E_{miss} distributions in the b → $\tau^-\bar{\nu}_\tau$X and b → $\tau^-\bar{\nu}_\tau$D$^{*\pm}$X final states are displayed in Figs. 4a and 4b, for the data and for the re-weighted simulation (Sect. 4), normalized to the number of observed events.

Table 3. Numbers of events observed in the data at large $E_{\rm miss}$ in the $b \to \tau^- \bar{\nu}_\tau X$ and $b \to \tau^- \bar{\nu}_\tau D^{*\pm} X$ final states. Also indicated are the events expected from the various background and signal processes. For the latter, the fitted branching ratio value was assumed. The corresponding selection efficiencies are indicated in brackets

Final state selection	$\tau^- \bar{\nu}_\tau X$	$\tau^- \bar{\nu}_\tau D^{*\pm} X$
$E_{\rm miss}$ interval	[18,35] GeV	[12,35] GeV
Data		
Hemispheres selected	2094	162
Expected background (details)		
u, d, s	17	2
b, c with leptonic decay	1001	51
$b \to D_s^- X$, $D_s^- \to \tau^- \bar{\nu}_\tau$	214	–
b, c without ℓ, D_s^-	84	36
Expected signal (details)		
$b \to \tau^- \bar{\nu}_\tau X$	(2%) 778	–
$b \to \tau^- \bar{\nu}_\tau D^{*\pm} X$	–	(0.26%) 63
$b \to \tau^- \bar{\nu}_\tau X$ without$D^{*\pm}$	–	10

5.1 Branching ratio extraction

An excess of events at large $E_{\rm miss}$ is indeed observed over the background in both distributions. The corresponding branching ratios were extracted with a binned-likelihood fit of the expected to the observed missing-energy distributions, keeping the normalization to the number of events observed. The fit was performed in $E_{\rm miss}$ intervals chosen so as to *(i)* minimize their total uncertainty, defined as the quadratic sum of the statistical and the systematic contributions (Sect. 5.2); and *(ii)* make the measurements statistically independent of that of the $B^- \to \tau^- \bar{\nu}_\tau$ branching fraction. The optimal intervals, indicated in Fig. 4, are found to be 18-35 GeV and 12-35 GeV, respectively.

The numbers of events in these intervals, observed in the data and expected from both the background and the signal processes, are displayed in Table 3. In particular, the cascade decay $b \to D_s^- X$ with $D_s^- \to \tau^- \bar{\nu}_\tau$, which yields an $E_{\rm miss}$ spectrum similar to that of the decay $b \to \tau^- \bar{\nu}_\tau X$, is included in the backgrounds to this signature.

These numbers yield measured branching fractions of

$$\begin{aligned}&{\rm BR}(b \to \tau^- \bar{\nu}_\tau X)\\ &\quad = [2.43 \pm 0.20({\rm stat.}) \pm 0.25({\rm syst.})]\,\%,\\ &\text{and}\\ &{\rm BR}(b \to \tau^- \bar{\nu}_\tau D^{*\pm} X)\\ &\quad = [0.88 \pm 0.31({\rm stat.}) \pm 0.28({\rm syst.})]\,\%,\end{aligned}$$

in agreement with the standard model predictions of $(2.30 \pm 0.25)\%$ and approximately 1%, respectively. The systematic uncertainties, also indicated above, are discussed in the next section.

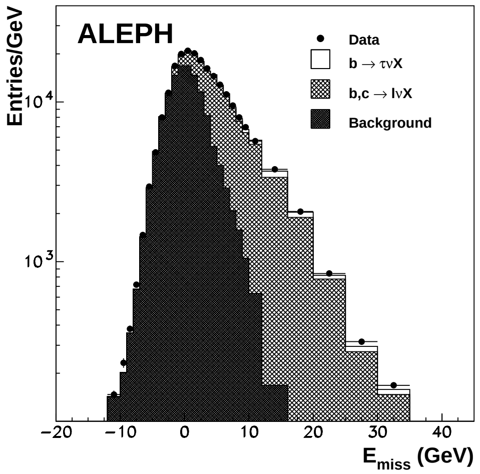

Fig. 5. $E_{\rm miss}$ distributions obtained for the data (dots) and the simulation (histogram) from the selection described in Sect. 3.2 with the lepton-veto criteria reversed

5.2 Systematic uncertainties

The measured branching ratios BR($b \to \tau^- \bar{\nu}_\tau X$) and BR($b \to \tau^- \bar{\nu}_\tau D^{*\pm} X$) can be affected by several sources of systematic effects on the signal selection efficiencies and by residual inaccuracies of the background simulation. The relevant sources common to $b \to \tau^- \bar{\nu}_\tau X$ and $b \to \tau^- \bar{\nu}_\tau D^{*\pm} X$ are addressed in turn below, and their effects on the branching fractions are summarized in Table 4.

1. The missing-energy distributions of $b \to \tau^- \bar{\nu}_\tau X$ and $b, c \to \ell \nu_\ell X$ depend on the experimentally determined quantities $\langle x_{\rm b} \rangle$, $\langle x_{\rm c} \rangle$, BR($b \to \ell \nu_\ell X$) and BR($b \to c \to \ell \nu_\ell X$). However, the small, residual differences between the $E_{\rm miss}$ distributions in the data and the simulation, obtained by reversing the lepton-veto criteria (Fig. 5), were found to be well accounted for by the measured uncertainties on their values. The whole extraction procedure of the branching fractions was therefore repeated by varying these quantities within their uncertainties, so as to evaluate the corresponding systematic effects. Similarly, the branching ratio dependence on the D^{**} content in b decays was accounted for according to [25].
2. The b-fragmentation modelling affects the b-energy spectrum, and therefore also the missing-energy spectrum in $b \to \tau^- \bar{\nu}_\tau X$ and $b, c \to \ell \nu_\ell X$. The effect of its knowledge was estimated in a similar manner by using the four different fragmentation functions described in [26], adjusted to reproduce the measured value of $\langle x_{\rm b} \rangle$. The corresponding systematic uncertainty was defined as the largest change in the measured branching fractions.
3. The $\bar{\nu}_\tau$ energy spectrum in the b rest frame also depends on whether it is computed with HQET or with the spectator model [1]. To reflect this difference, the neutrino spectrum was distorted with a weight depending linearly on the neutrino energy such that the

Table 4. Systematic uncertainties (in %) for BR($\mathrm{b} \to \tau^- \bar{\nu}_\tau \mathrm{X}$) and BR($\mathrm{b} \to \tau^- \bar{\nu}_\tau \mathrm{D}^{*\pm} \mathrm{X}$)

Source	BR($\mathrm{b} \to \tau^- \bar{\nu}_\tau \mathrm{X}$)	BR($\mathrm{b} \to \tau^- \bar{\nu}_\tau \mathrm{D}^{*\pm} \mathrm{X}$)
$\langle x_\mathrm{b} \rangle$=0.702 ± 0.008 [28]	∓0.12	∓0.15
$\langle x_\mathrm{c} \rangle$=0.487 ± 0.008 [28]	∓0.01	∓0.01
BR($\mathrm{b} \to \ell \nu_\ell \mathrm{X}$)=10.56 ± 0.21 %[29]	∓0.05	∓0.10
BR($\mathrm{b} \to \mathrm{c} \to \ell \nu_\ell \mathrm{X}$)=7.98 ± 0.22%[29]	∓0.01	∓0.03
BR($\mathrm{b} \to \mathrm{D}^{**}, \mathrm{D}^{*\pm}\pi$) =25 ± 7%[25]	±0.03	±0.06
b-fragmentation modelling [26]	∓0.11	∓0.12
$\mathrm{b} \to \tau^- \bar{\nu}_\tau \mathrm{X}$ decay modelling	±0.06	±0.06
BR($\mathrm{D}_\mathrm{s}^\pm \to \tau^\pm \nu_\tau$)=5.79 ± 1.94%[27]	∓0.08	∓0.07
$\langle \mathrm{P}_\tau \rangle = -0.735 \pm 0.03$ [1]	±0.02	±0.01
$\langle \mathrm{P}(\Lambda_\mathrm{b}) \rangle = -0.31^{+0.22}_{-0.19} \pm 0.08$ [24]	∓0.06	∓0.01
b-tagging efficiency	±0.06	±0.02
μ-identification efficiency	±0.06	±0.07
e-identification efficiency	±0.08	±0.08
Visible-energy calibration	∓0.05	∓0.04
E_miss in $\mathrm{b\bar{b}}$ events	±0.06	±0.05
Combinatorial background	–	±0.03
Total systematic uncertainty	±0.25	±0.28

averaged energy changes by ±10%, and the resulting change in the measured branching fractions noted.

4. The ν_τ energy spectrum depends on the τ polarization and, for events containing a Λ_b, on the Λ_b polarization. These polarizations were varied according to the measured uncertainty on the latter, and to the difference between the HQET and the spectator model prediction for the former, to determine their effects on the branching fractions.
5. The uncertainty on $\mathrm{b} \to \mathrm{D}_\mathrm{s}^- \mathrm{X}$, followed by $\mathrm{D}_\mathrm{s}^\pm \to \tau^\pm \nu_\tau$ [27] was propagated to the branching fractions. In this process, the missing-energy spectrum is expected to be similar to that of the signal.
6. The small, residual differences between the calibrated missing-energy distributions for light-quark events, the b-tagging efficiencies and the lepton-veto effectiveness in data and simulation (Sect. 4) were all attributed to systematic effects and translated as such to the branching fraction determination.
7. The visible-energy calibration procedure (Sect. 4.1) is tuned with light-quark events, and may not be entirely accurate for $\mathrm{b\bar{b}}$ events in the signal region. In this region, the missing energy is found in the simulation to mainly originate from mis-reconstructed neutral hadrons. It is observed that $\mathrm{b\bar{b}}$ events yield more hemispheres with a large neutral hadronic energy in the data than in the simulation. This excess is expected to increase the residual background in the signal region by $\sim 20\%$, treated as an additional systematic uncertainty.

Two additional systematic effects, specific to the $\mathrm{b} \to \tau^- \bar{\nu}_\tau \mathrm{D}^{*\pm} \mathrm{X}$ final state were also identified. First, the combinatorial background was estimated in that case from the sidebands around the D^0 peak, and used to derive the corresponding uncertainty on BR($\mathrm{b} \to \tau^- \bar{\nu}_\tau \mathrm{D}^{*\pm} \mathrm{X}$). Second, the b-tagging criterion specific to this channel (Sect. 3.4) yields a different efficiency in data and simulation, which affects BR($\mathrm{b} \to \tau^- \bar{\nu}_\tau \mathrm{D}^{*\pm} \mathrm{X}$).

6 Upper limits on $\mathrm{B}^- \to \tau^- \bar{\nu}_\tau$ and $\mathrm{b} \to \mathrm{s}\nu\bar{\nu}$

The $\mathrm{B}^- \to \tau^- \bar{\nu}_\tau$ and $\mathrm{b} \to \mathrm{s}\nu\bar{\nu}$ branching ratios are predicted to be too small in the standard model to be measured with only four million hadronic Z decays. However, upper limits can be set on these branching fractions to constrain possible extensions of the standard model, such as type-II two-Higgs-doublet models. Since BR($\mathrm{B}^- \to \tau^- \bar{\nu}_\tau$) and BR($\mathrm{b} \to \mathrm{s}\nu\bar{\nu}$) can be affected differently depending on the new physics considered, the upper limits are conservatively estimated here for each process separately.

The missing-energy distribution of the events selected as described in Sect. 3.3 is displayed in Fig. 6, and is compared to that of the background. Also indicated in Fig. 6 is the expected enhancement at large missing energy, should either the $\mathrm{B}^- \to \tau^- \bar{\nu}_\tau$ or the $\mathrm{b} \to \mathrm{s}\nu\bar{\nu}$ branching ratio be 1%.

No background subtraction was performed, making the validity of the results presented here unaffected by possible systematic uncertainties related to the knowledge of the residual background, largely suppressed by a lower

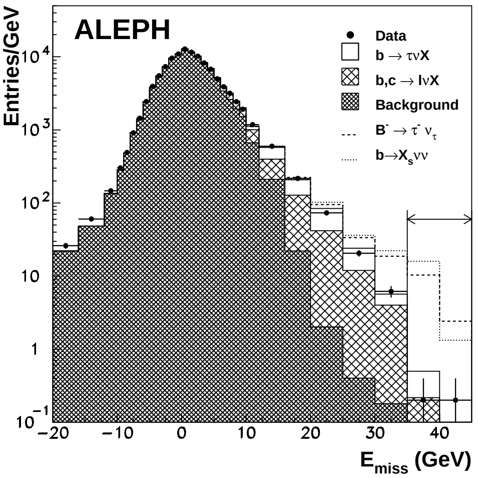

Fig. 6. Missing-energy distributions in the $B^- \to \tau^- \bar{\nu}_\tau$ and $b \to s\nu\bar{\nu}$ final state selection, for the data (dots) and for the simulated background (full histogram). Also indicated are the contributions of the $B^- \to \tau^- \bar{\nu}_\tau$ (dashed histogram) and $b \to s\nu\bar{\nu}$ (dotted histogram) processes with a branching ratio of 1%. The arrow shows the region in which the two limits are calculated

Table 5. Numbers of events observed in the data in three different E_{miss} intervals. Also indicated are the events expected from the various background and signal processes. For the latter, a branching ratio of 1% was assumed

E_{miss} interval	[30, 35] GeV	[35, 40] GeV	> 40 GeV
Data			
Selected hemispheres	31	1	1
Simulation			
Expected hemispheres	37.0±2.7	2.5 ± 1.6	< 1
Background (detail)			
$b \to \tau^- \bar{\nu}_\tau X$	7.2	1.4	–
b, c with leptonic decay	28.9	1.1	–
Other Backgrounds	0.9	–	–
Signal (BR=1%)			
$B^- \to \tau^- \bar{\nu}_\tau$	76.9	53.1	12.7
$b \to s\nu\bar{\nu}$	91.0	78.6	6.6

cut on the missing energy at 35 GeV. The latter cut was optimized so as to maximize the expected 90% C.L. upper limit, evaluated with simple event counting and in the absence of new physics [30], on the $B^- \to \tau^- \bar{\nu}_\tau$ and $b \to s\nu\bar{\nu}$ branching ratios. The numbers of events, observed in the data and expected from background and signal, are displayed in Table 5 in three missing-energy intervals. Two events with a missing energy in excess of 35 GeV were observed, with 2.5 ± 1.6 events expected from all background processes. In absence of any systematic uncertainty, the 90% C.L. upper limits on the $B^- \to \tau^- \bar{\nu}_\tau$ and $b \to s\nu\bar{\nu}$ branching fractions are found to be 8.1×10^{-4} and 6.2×10^{-4}, respectively.

However, these limits are affected by the uncertainty on the expected fraction of $B^- \to \tau^- \bar{\nu}_\tau$ and $b \to s\nu\bar{\nu}$ events with such a large missing energy or, almost equivalently, with such a large value of x_{b}. (Most of these events are characterized by a value of x_{b} in excess of 0.9.) This fraction was determined [31] to be $0.146^{+0.025}_{-0.021}$, which translates to an uncertainty of 15% on the number of events expected. In addition, the fraction of B^- in $Z \to b\bar{b}$ events is known [32] to be (38.9 ± 1.3)%. The latter uncertainty of 3% on the number of events expected affects only the limit on the $B^- \to \tau^- \bar{\nu}_\tau$ branching ratio. These two uncertainties were taken into account following the method of [33], yielding the limits

$$\mathrm{BR}(B^- \to \tau^- \bar{\nu}_\tau) < 8.3 \times 10^{-4},$$
$$\mathrm{BR}(b \to s\nu\bar{\nu}) < 6.4 \times 10^{-4},$$

at the 90% confidence level.

7 Measurement of BR($b \to \tau^- \bar{\nu}_\tau X$) with di-leptons

An alternative method of measuring BR($b \to \tau^- \bar{\nu}_\tau X$) was developed with events where both the τ and the accompanying D decay to e or μ. Hence, the signature used to tag the signal events is a pair of leptons (e, μ) of opposite sign in a jet. The background, originating from $b \to c\ell^- \bar{\nu}_\ell$ followed by $c \to q\ell^+ \nu_\ell$, is about 20 times larger than the signal. Signal and background are therefore separated on the basis of their different kinematic properties. Although this method is statistically less powerful than that based on missing energy, it represents an interesting cross-check since it is based on a complementary sample of events and sources of systematic uncertainties are largely different. Indeed, the main contribution to the systematic error comes from the uncertainty on the product BR($b \to \ell \bar{\nu}_\ell c$, $c \to \ell \nu_\ell q$) and on the double charm decay rates, $B \to D_s D(X)$ and $B \to D^0 D(X)$.

The presence of three neutrinos in the decay chain of signal events is the main difference between signal and background. As a consequence, $b \to \tau^- \bar{\nu}_\tau X$ decays give larger missing energy, softer lepton spectrum and smaller charged multiplicity to the jet containing the lepton candidates. These different kinematic properties of the various categories of events are used to separate the signal from the background. A multivariate analysis technique with a multilayered neural network (NN) is used to obtain the best discriminating power.

7.1 Event selection

Electron and muon identification follows the standard criteria [17], with two refinements for muons. Firstly, the muon momentum cut is lowered from 3 GeV/c to 2.2 GeV/c to increase the acceptance for the signal (2.2 GeV/c is the minimum momentum for a muon to reach the muon chambers) and secondly, any track "shadowed" by another track is rejected in the di-lepton selection. Two tracks are said to be shadowing if they share in common either hits in the last ten layers of the hadron calorimeter or at least one three-dimensional muon chamber hit. This latter cut allows a good description of the background to be obtained in the sample of events with two muons in the same jet, as shown in [34]. To obtain the di-lepton sample used for the training of the neural network, two additional cuts on the invariant mass $M_{\ell\ell}$ of the lepton pair are applied.

- Electron pair invariant masses are required to be greater than $0.3\,\mathrm{GeV}/c^2$ in order to reject γ conversions or Dalitz decays of η, π^0.
- Electron pairs and muon pairs are required to have an invariant mass smaller than $2.5\,\mathrm{GeV}/c^2$ to avoid pairs coming from J/ψ decays.

After these selection cuts, the simulated di-lepton sample consists of 451 signal events, 7834 $\mathrm{b} \to \ell$ background events and 5249 di-leptons coming from hadrons mis-identified as leptons and light-hadron decays.

7.2 Analysis method and background estimation

Jets are reconstructed by the JADE clustering algorithm [35] with a y_{cut} of 0.0044 [17]. The following variables are selected as input to the NN: the missing energy in the hemisphere of the jet containing the lepton pair, the momenta of the leptons boosted to the reconstructed b-hadron rest frame [34], the invariant mass of the lepton pair, the transverse momenta of the leptons with respect to the jet direction, the total energy and the charged energy of the jet containing the lepton pair, the fraction of the jet charged energy carried by the leptons and the number of charged particles in the jet.

The main background consists of di-leptons coming from $\mathrm{b} \to \mathrm{c}\ell$, $\mathrm{c} \to \ell' \nu_{\ell'}$ decays. To determine the product $\mathrm{BR}(\mathrm{b} \to \ell \bar{\nu}_\ell \mathrm{c}) \times \mathrm{BR}(\mathrm{c} \to \ell' \nu_{\ell'})$, the semi-leptonic branching fraction $\mathrm{BR}(\mathrm{b} \to \ell \bar{\nu}_\ell \mathrm{X})$ is fixed to the LEP average value [29], while the $\mathrm{b} \to \mathrm{c} \to \ell'$ fraction is determined from the same sample of di-lepton events as follows: a neural network with the input variables described above is trained to separate $\mathrm{b} \to \mathrm{c}\ell \to \ell\ell'\mathrm{X}$ decays from all other processes; and the $\mathrm{b} \to \mathrm{c} \to \ell$ fraction is extracted by fitting the simulated neural network output distribution to that of the data. No attempt at an evaluation of the systematic uncertainties on this fraction was made.

Another important background consists of leptons from light-hadron decays or of hadrons mis-identified as leptons. A control sample of same sign di-leptons is used to test the accuracy of the simulation. This sample has a composition similar to that of the background of the analysis, since one lepton candidate is always fake or coming from the decay of a light-flavoured hadron.

The measured values [36] for double charmed b decays ($\mathrm{B} \to \mathrm{D_s D(X)}$, $\mathrm{B} \to \mathrm{D^0 D(X)}$) are included in the background estimate as well.

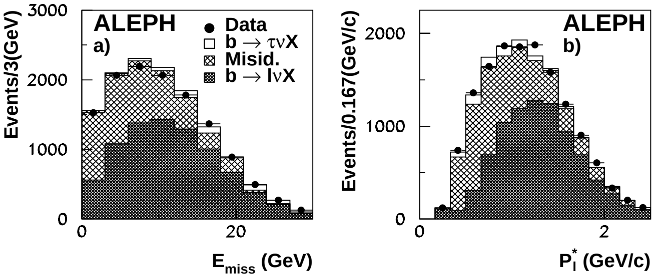

Fig. 7a,b. Data and normalized Monte Carlo distributions for **a** the missing energy of the leptonic hemisphere and **b** the momentum of one lepton boosted to the reconstructed b-hadron rest frame. The normalization of the simulated distribution for signal events corresponds to the $\mathrm{BR}(\mathrm{b} \to \tau^- \bar{\nu}_\tau \mathrm{X})$ value obtained from the fit

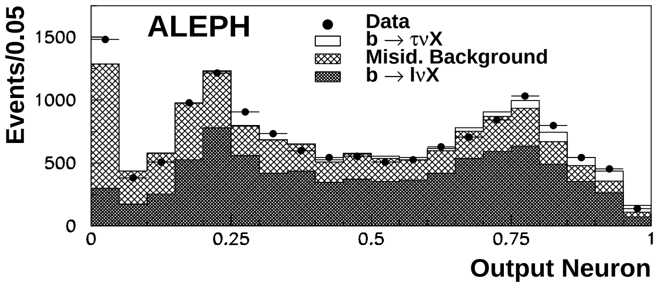

Fig. 8. Output neuron distributions for data and simulation (histograms). The normalization of the simulation $\mathrm{BR}(\mathrm{b} \to \tau^- \bar{\nu}_\tau \mathrm{X})$ distribution corresponds to the branching fraction value obtained from the fit. The samples labelled $\mathrm{b} \to \tau^- \bar{\nu}_\tau \mathrm{X}$ and $\mathrm{b} \to \ell \bar{\nu}_\ell \mathrm{X}$ in the figure contain only the events where both leptons are correctly identified. Events with at least one lepton mis-identified are classified as "Mis-identification background"

7.3 Branching ratio estimation with a neural network

The agreement between data and Monte Carlo distributions is good for all the variables used in the analysis. An example is shown in Fig. 7 for two of these variables. The sample of simulated events is rescaled so that the number of selected hadronic events is equal to that in the data. The value of $\mathrm{BR}(\mathrm{b} \to \tau^- \bar{\nu}_\tau \mathrm{X})$ is obtained by fitting the simulated output neuron distribution to the observed distribution, shown in Fig. 8. The discrepancy in the first bin has been traced, using the same sign di-lepton sample, to a subset of mis-identified muons not well reproduced by the simulation [34]. These background events are well separated from the signal events by the NN. The inclusion of the first bin in the fit has a negligible effect on the fitted branching fraction.

The dominant contributions to the systematic errors are the uncertainties in the values of the branching ratios involved in the analysis, the uncertainties in the modelling of semi-leptonic decays, the effect of the E_{miss} calibration previously discussed and those inherent to the lepton identification. Some sources of systematic uncertainty (such as those related to the lepton identification) which affect both $\mathrm{b} \to \tau^- \bar{\nu}_\tau \mathrm{X}$ and $(\mathrm{b} \to \mathrm{c} \to \ell)$ are properly taken into account. All the errors were obtained by varying the amount of the component of the event sample under study according to its uncertainty, changing the distribution of their input variables to the NN when required, and re-fitting the NN output neuron. The changes in the fitted fraction of $b \to \tau^- \bar{\nu}_\tau X$ events and in BR($b \to c \to \ell$) are evaluated with their respective NN, and the corresponding change in the BR($b \to \tau^- \bar{\nu}_\tau X$) is calculated.

The result is

$$\mathrm{BR}(b \to \tau^- \bar{\nu}_\tau X) = [3.36 \pm 0.67\ (\mathrm{stat.})\ \pm 0.60\ (\mathrm{syst.})]\,\%.$$

Various consistency checks are performed. The lepton identification performance are tested by obtaining results separately for the three subsamples of di-electrons ($e^\pm, e^\mp$), di-muons ($\mu^\pm, \mu^\mp$) and ($e^\pm, \mu^\mp$) pairs. The measured branching fractions BR($b \to \tau^- \bar{\nu}_\tau X$) are found to be ($3.8 \pm 1.3$)%, ($3.6 \pm 1.4$)% and ($2.9 \pm 1.0$)%, respectively. The simulation of the missing energy is tested in two ways. First, a NN fed with charged track information only gives BR($b \to \tau^- \bar{\nu}_\tau X$) =($3.15 \pm 0.89$)%. Second, the branching fraction obtained when fitting the E_{miss} distribution instead of the NN output is (3.05 ±0.90)%.

8 Interpretation in two-Higgs-doublet models

As discussed in Sect. 1, all five measurements presented in this paper can in principle be used to constrain type-II two-Higgs-doublet models. Practically, however, the constraints obtained in this framework are largely dominated by two of these measurements.

- The Z penguin diagrams (Fig. 1f) are related to photon penguin diagrams already severely constrained by $b \to s\gamma$ searches, and cannot contribute significantly to $b \to s\nu\bar{\nu}$[8].
- The BR($b \to \tau^- \bar{\nu}_\tau D^{*\pm} X$) measurement is significantly correlated with, and is statistically less powerful than that of BR($b \to \tau^- \bar{\nu}_\tau X$).
- The BR($b \to \tau^- \bar{\nu}_\tau X$) measurement with di-leptons is much less accurate than the corresponding measurement based on missing energy.

Consequently, only the BR($b \to \tau^- \bar{\nu}_\tau X$) measurement based on missing energy and the search for the $B^- \to \tau^- \bar{\nu}_\tau$ final state, kept statistically independent in the analysis, were interpreted to constrain type-II two-Higgs-doublet models. In these models, both branching ratios depend on the parameter r,

$$r \equiv \frac{\tan\beta}{m_{H^\pm}},$$

where $\tan\beta$ is the ratio of the vacuum expectations values of the two Higgs doublets, and $m_{H^\pm}$ is the mass of the resulting charged Higgs boson. In the free-quark model, the $b \to \tau^- \bar{\nu}_\tau X$ branching ratio is expected to be modified with respect to the standard model prediction according to [2]

$$\begin{aligned}&\mathrm{BR}(b \to \tau^- \bar{\nu}_\tau X)\\ &= \mathrm{BR}^{\mathrm{SM}}(b \to \tau^- \bar{\nu}_\tau X) \times \left[1 - 2m_\tau^2 r^2 \Phi + \frac{m_\tau^2 m_b^2}{4} r^4\right], \end{aligned} \quad (3)$$

where Φ is a phase-space factor depending on m_τ, m_c and m_b amounting to about 0.6. An enhancement can therefore be observed for values of r in excess of $\sim 0.43\,(\mathrm{GeV}/c^2)^{-1}$, while the destructive interference yields a reduction of the branching ratio below that value. Similarly, the $B^- \to \tau^- \bar{\nu}_\tau$ fraction is modified with respect to the standard model by

$$\begin{aligned}&\mathrm{BR}(B^- \to \tau^- \bar{\nu}_\tau)\\ &\quad = \mathrm{BR}^{\mathrm{SM}}(B^- \to \tau^- \bar{\nu}_\tau) \times \left[1 - r^2 m_{B^-}^2\right]^2 .\end{aligned} \quad (4)$$

which shows an even stronger dependence on r, and represents an enhancement for all values of r larger than $\sim 0.27\,(\mathrm{GeV}/c^2)^{-1}$.

To extract a limit on r, the neutrino energy spectrum and the τ polarization were computed as a function of r [3], and the simulated events, generated with the standard model values, were re-weighted accordingly. The BR($b \to \tau^- \bar{\nu}_\tau X$) measurement and the BR($B^- \to \tau^- \bar{\nu}_\tau$) limit were derived as presented in Sects. 5 and 6, for any r value.

From the dependence between BR($b \to \tau^- \bar{\nu}_\tau X$) and r of (3), and from the value of BR$^{\mathrm{SM}}$($b \to \tau^- \bar{\nu}_\tau X$), a 90% C.L. upper limit on r was extracted [3,4,38]:

$$\tan\beta / m_{H^\pm} < 0.49\,\left(\mathrm{GeV}/c^2\right)^{-1} \ \text{at 90\% CL.} \quad (5)$$

The τ polarization actually plays here an important rôle since, for $r = 0.49\,(\mathrm{GeV}/c^2)^{-1}$, it amounts to -0.28 while the standard model prediction is -0.735 in $b \to \tau^- \bar{\nu}_\tau X$ decays. This effect had been neglected in previous ALEPH analyses [11].

The dependence between BR($B^- \to \tau^- \bar{\nu}_\tau$) and r of (4) and the standard model value of the branching ratio,

$$\begin{aligned}\mathrm{BR}^{\mathrm{SM}}(B^- \to \tau^- \bar{\nu}_\tau) &= 7.4 \times 10^{-5}\,(f_B/160\,\mathrm{MeV})^2\\ &\quad \times (|V_{ub}|/0.004)^2 ,\end{aligned}$$

were interpreted in terms of a 90% C.L. upper limit on r:

$$\tan\beta / m_{H^\pm} < 0.40\,\left(\mathrm{GeV}/c^2\right)^{-1} \ \text{at 90\% CL.} \quad (6)$$

In the limit extraction, the systematic uncertainties on f_B [39] and on V_{ub} [25] were taken into account following the method of [33]. The combination of the two results in (5) and (6) cannot improve on the latter, since the corresponding r value does not enhance the $b \to \tau^- \bar{\nu}_\tau X$ branching ratio.

9 Conclusion

With approximately four million hadronic Z decays collected by the ALEPH detector at LEP, branching ratios involving a $b \to \tau$ transition have been measured to be

$$\begin{aligned}\mathrm{BR}(b \to \tau^- \bar{\nu}_\tau X) &= (2.43 \pm 0.20 \pm 0.25)\%,\\ \mathrm{BR}(b \to \tau^- \bar{\nu}_\tau D^{*\pm} X) &= (0.88 \pm 0.31 \pm 0.28)\%,\end{aligned}$$

in agreement with the standard model predictions and consistent with similar measurements performed by DELPHI [40] and L3 [41,42]. A search for the exclusive decay $\mathrm{B}^- \to \tau^- \bar{\nu}_\tau$ has allowed a 90% C.L. upper limit to be set on the corresponding branching ratio,

$$\mathrm{BR}(\mathrm{B}^- \to \tau^- \bar{\nu}_\tau) < 8.3 \times 10^{-4} \text{ at } 90\% \text{ CL.}$$

Similar limits have been obtained by CLEO [43], L3 [44] and DELPHI [40]. In the framework of type-II two-Higgs-doublet models, these results translate to a constraint on the model parameter $r = \tan\beta / m_{\mathrm{H}^\pm}$,

$$\tan\beta / m_{\mathrm{H}^\pm} < 0.40 \left(\mathrm{GeV}/c^2\right)^{-1} \text{ at } 90\% \text{ CL.}$$

Finally, a limit has been set on the process $\mathrm{b} \to \mathrm{s}\nu\bar{\nu}$ to

$$\mathrm{BR}(\mathrm{b} \to \mathrm{s}\nu\bar{\nu}) < 6.4 \times 10^{-4} \text{ at } 90\% \text{ CL.}$$

A related limit on $\mathrm{BR}(\mathrm{B}^- \to \mathrm{K}^- \nu\bar{\nu})$ has been obtained by CLEO [43].

Acknowledgements. We would like to thank Yuval Grossman, Zoltan Ligeti and Enrico Nardi for fruitful discussions on the $\mathrm{b} \to \mathrm{s}\nu\bar{\nu}$ process and the computation of the limit on $\tan\beta / m_{\mathrm{H}^\pm}$ in the $\mathrm{b} \to \tau^- \bar{\nu}_\tau \mathrm{X}$ channel. We are indebted to our colleagues in the accelerator divisions for the good performance of LEP. We thank also the engineers and technicians of all our institutions for their contribution to the excellent performance of ALEPH. Those of us from non-member countries thank CERN for its hospitality.

References

1. A. Falk et al., Heavy quark expansion for the inclusive decay $b \to \tau\bar{\nu}_\tau X$, Phys. Lett. **B326** (1994) 145
2. J. Kalinowski, Semi-leptonic decays of B mesons into $\tau\nu_\tau$ in a two Higgs doublet model, Phys. Lett. **B245** (1990) 201
3. Y. Grossman, Z. Ligeti, The inclusive $b \to \tau\bar{\nu}_\tau X$ decay in two Higgs doublet models, Phys. Lett. **B332** (1994) 373
4. Y. Grossman, H.E. Haber, Y. Nir, QCD corrections to charged Higgs-mediated $b \to c\tau\nu_\tau$ decay, Phys. Lett. **B357** (1995) 630
5. J.C. Körner, G.A. Schuler, Exclusive semileptonic heavy meson decays including lepton mass effects, Z. Phys. C (1990) 93
6. B. Grzadkowski, Wei-Shu Hou, Searching for $B \to D\tau\nu$ at the 10% level, Phys. Lett. **B283** (1992) 427
7. Wei-Shu Hou, Enhanced charged Higgs boson effects in $B \to \tau\nu, \mu\nu$ and $b \to \tau\bar{\nu}_\tau X$, Phys. Rev. **D48** (1993) 2342
8. Y. Grossman, Z. Ligeti, E. Nardi, First limit on inclusive $B \to X_s\nu\nu$ decay and constraints on new physics, Nucl. Phys. **B465** (1996) 369
9. Y. Grossman, Z. Ligeti, E. Nardi, First limit on inclusive $B \to X_s\nu\nu$ decay and constraints on new physics (Erratum), Nucl. Phys. **B480** (1996) 753
10. ALEPH Collaboration, Measurement of the $b \to \tau\bar{\nu}_\tau X$ branching ratio, Phys. Lett. **B298** (1993) 479
11. ALEPH Collaboration, Measurement of the $b \to \tau\bar{\nu}_\tau X$ branching ratio and an upper limit on $\mathrm{BR}(B^- \to \tau\bar{\nu}_\tau)$, Phys. Lett. **B343** (1995) 444
12. ALEPH Collaboration, ALEPH: a detector for electron-positron annihilations at LEP, Nucl. Instrum. and Methods **A294** (1990) 121
13. ALEPH Collaboration, Performance of the ALEPH detector at LEP, Nucl. Instrum. and Methods **A360** (1995) 481
14. ALEPH Collaboration, A precise measurement of $\Gamma(Z \to b\bar{b})/\Gamma(Z \to \text{hadrons})$, Phys. Lett. **B313** (1993) 535
15. ALEPH Collaboration, Determination of the number of light neutrino species, Phys. Lett. **B231** (1989) 519
16. ALEPH Collaboration, Measurement of the B_s^0 lifetime, Phys. Lett. **B322** (1994) 275
17. ALEPH Collaboration, Heavy-quark tagging with leptons in the ALEPH detector, Nucl. Instrum. and Methods **A346** (1994) 461
18. ALEPH Collaboration, Production of charmed mesons in Z decays, Z. Phys. **C62** (1994) 1
19. T. Sjöstrand, M. Bengtsson, The LUND Monte Carlo for jet fragmentation and e^+e^- physics, Comp. Phys. Commun. **43** (1987) 367
20. T. Sjöstrand, High-energy physics event generation with PYTHIA 5.7 and JETSET 7.4, Comp. Phys. Commun. **82** (1994) 74
21. GEANT: Detector description and simulation tool, CERN program library long write-up W5013, Application Software Group, IT Division, CERN
22. A. Ali, T. Mannel, Exclusive rare B-decays in the heavy-quark limit, Phys. Lett. **B264** (1991) 447; Erratum **B274** (1992) 526
23. S. Jadach, J.H. Kühn, Z. Wąs, The Monte Carlo program KORALZ version 3.8 for the lepton or quark pair production at LEP/SLC energies, Comp. Phys. Commun. **64** (1991) 275; Comp. Phys. Commun. **66** (1991) 276
24. ALEPH Collaboration, Measurement of the Λ_b polarization in Z decays, Phys. Lett. **B365** (1996) 437
25. ALEPH, CDF, DELPHI, L3, OPAL and SLD Collaborations, Combined results on b-hadron production rates, lifetimes, oscillations, and semileptonic decays, CERN-EP/2000-096 (2000)
26. The LEP Electroweak Working Group, Presentation of LEP EW HF results for the summer 1994 conferences, LEPHF/94-02
27. N. Marinelli, Leptonic decays of the D_s meson at LEP, Proceedings of ICHEP2000, 27-Jul/02-Aug-2000, Osaka, Japan, submitted to World Scientific
28. The LEP Heavy Flavour Working Group, Input parameters for the LEP/SLD EW HF results for the summer 1998 conferences, LEPHF/98-01
29. S. C. Blyth, Inclusive b-hadron semileptonic decays at LEP and extraction of $|V_{cb}|$, Proceedings of ICHEP2000, 27-Jul/02-Aug-2000, Osaka, Japan, submitted to World Scientific
30. ALEPH Collaboration, Search for the standard model Higgs boson, Phys. Lett. **B313** (1993) 299; J.-F. Grivaz and F. Le Diberder, Complementary analyses and acceptance optimization in new particle searches, LAL 92-37 (1992)
31. ALEPH Collaboration, Measurement of the effective b-quark fragmentation function at the Z resonance, Phys. Lett. **B357** (1995) 699

32. ALEPH Collaboration, An investigation of B_d^0 and B_s^0 oscillation, Phys. Lett. **B322** (1994) 441
33. R.D. Cousins, V.L. Highland, Nucl. Instrum. and Methods **A320** (1992) 331
34. Anna Pascual, Measurement of the Inclusive Semi-leptonic Branching Fraction $BR(b \to \tau\bar{\nu}_\tau X)$ using the ALEPH detector, PhD Thesis, Universitat Autònoma de Barcelona (1995)
35. JADE Collaboration, Experimental studies on multijet production in e^+e^- annihilations at PETRA energies, Z. Phys. **C33** (1986) 23
36. ALEPH Collaboration, Observation of doubly-charmed B decays at LEP, Eur. Phys. J. **C4** (1998) 387
37. ALEPH Collaboration, Heavy flavour production and decay with prompt leptons in the ALEPH detector, Z. Phys. **C62** (1994) 179
38. Y. Grossman, Z. Ligeti, Private communication
39. C. Bernard et al. (MILC Collaboration), Lattice determination of heavy-light decay constants, Phys. Rev. Lett. **81** (1998) 4812
40. DELPHI Collaboration, Upper limit for the decay $B^- \to \tau\bar{\nu}_\tau$ and measurement of the $b \to \tau\bar{\nu}_\tau X$ branching ratio, CERN-EP/99-162 (1999)
41. L3 Collaboration, Measurement of the inclusive $b \to \tau\bar{\nu}_\tau X$ branching ratio, Phys. Lett. **B332** (1994) 201
42. L3 Collaboration, Measurement of the Branching Ratios $b \to e\nu X$, $\mu\nu X$, $\tau\nu X$ and νX, Z. Phys. **C71** (1996) 379
43. CLEO Collaboration, A search for $B \to \tau\nu$, hep-ex/007057, submitted to Phys. Rev. Lett
44. L3 Collaboration, Measurement of $D_s \to \tau\nu$ and a new limit for $B \to \tau\nu$, Phys. Lett. **B396** (1997) 327